ELSEVIER

Contents lists available at ScienceDirect

Journal of Inorganic Biochemistry

journal homepage: www.elsevier.com/locate/jinorgbio





Metal (Au, Pt, Pd, Ni) Bis(dithiolene) complexes as dual-action agents combating cancer and trypanosomatid infections

Hadi Hachem^a, Yann Le Gal^a, Olivier Jeannin^a, Dominique Lorcy^{a,*}, Gonzalo Scalese^b, Leticia Pérez-Díaz^c, Dinorah Gambino^{b,*}, António P. Matos^d, Fernanda Marques^{e,*}

- ^a Univ Rennes, CNRS, ISCR (Institut des Sciences Chimiques de Rennes) UMR 6226, F-35000 Rennes, France
- b Área Química Inorgánica, Departamento Estrella Campos, Facultad de Química, Universidad de la República, 11800 Montevideo, Uruguay
- ^c Sección Genómica Funcional, Instituto de Química Biológica, Facultad de Ciencias, Universidad de la República, 11400 Montevideo, Uruguay
- d Egas Moniz School of Health and Science, Egas Moniz Center for Interdisciplinary Research (CiiEM), University Campus, Quinta da Granja, Monte de Caparica, 2829-511 Caparica, Portugal
- ^e Centro de Cièncias e Tecnologias Nucleares and Departamento de Engenharia e Cièncias Nucleares, Instituto Superior Técnico, Universidade de Lisboa, Estrada Nacional 10, 2695-066 Bobadela LRS, Portugal

ARTICLE INFO

Keywords: Metal bis(dithiolene) complexes Electroactivity Structural modification Anticancer activity Antitrypanosomatid agent ROS production

ABSTRACT

Cancer and infection diseases pose severe threats to public health worldwide stressing the need for more effective and efficient treatments. Thus, the search for broad-spectrum activity drugs seems justifiable and urgent. Herein, we investigate the anticancer and antitrypanosomatid (anti-Trypanosoma cruzi) activities of eight monoanionic metal bis(dithiolene) complexes, $[Ph_4P][M(R-thiazdt)_2]$ with $M^{n+} = Au^{3+}$, Pt^{2+} , Pd^{2+} , Ni^{2+} , containing N-alkyl-1,3-thiazoline-2-thione dithiolene ligands (R-thiazdt) with different alkyl groups (R = Et, tBu). Compared to auranofin (AF) and cisplatin (CP), two reference drugs in clinical use, all complexes showed high anticancer activities against A2780 ovarian cancer cells (IC₅₀ values of 0.6–3.8 μM) some also being able to overcome CP resistance in A2780cisR cells. The selectivity index (SI), the IC50 values on normal cells (HDF) vs. A2780 cells, indicated good anticancer specificity (SI > 3) for most of the complexes but with clinical relevance for [Ph₄P][Pd (tBu-thiazdt)₂] (SI = 10). All complexes showed relevant antitrypanosomatid activities (IC₅₀ values of 2.6-5.8 μ M) some even exhibiting lower IC₅₀ values than the reference drug nifurtimox (NFX). The mechanism of cell death seemed to be mediated mainly by the formation of reactive oxygen species (ROS), although to lesser extent for the gold complexes but superior to AF. Although ROS play a role in the main apoptotic pathways, cell death by apoptosis was not evident as shown by the caspase-3/7 assay and the morphological cell features studies by electron microscopy (SEM). Results obtained evidenced that [Ph4P][Pt(tBu-thiazdt)2] and [Ph4P][Pd(tBu-thiazdt)2] thiazdt)2] complexes might have potential as novel anticancer and antitrypanosomatid agents as alternatives to current therapeutics.

1. Introduction

Coordination complexes have attracted increasing interest in the biomedical field for both therapeutic and diagnostic applications in a plethora of diseases offering different properties and alternative modes of action. In fact, their properties can be tuned depending on the metal chosen, its oxidation state and the number and type of coordinating ligands. The therapeutic applications of metal-based complexes have been an exciting area of research and deserves to be further explored in the search for novel therapeutic agents [1,2]. Within the arsenal of anticancer agents, metal-based complexes have made a significant contribution. Platinum-based compounds, specifically cisplatin (CP) and

analogues are widely used in the clinic for the treatment of several cancers [3]. Nearly 50 % of cancer patients, who undergo chemotherapy, receive a platinum drug either alone or in combination therapy. Although highly efficacious, treatment with CP is still limited by lack of selectivity, high systemic toxicity and drug resistance, which has been partially ameliorate by the introduction of new Pt(II) drugs [4]. These findings have prompted a great interest in the development of other metal complexes containing ions such as copper, iron, ruthenium and gold that have shown potent cytotoxic and antitumor effects [5]. Unlike to platinum drugs, these complexes are often relying on DNA-independent mechanisms such as targeting tumor-associated proteins and induction of oxidative stress for their anticancer effects. Notably, a

^{*} Corresponding author.

few of these drugs have already been evaluated as therapeutic candidates [6–8].

In the search for metal complexes other than CP and analogues, gold complexes have shown great promise for the treatment of several human diseases including cancer [9]. Auranofin (AF), a gold(I) complex, approved by FDA for the treatment of rheumatoid arthritis exhibits antiproliferative activity against various types of cancers. The phosphane and thiolate ligands in AF stabilise the gold(I) centre, and in view of that new analogues have been designed to improve the efficacy of such compounds [10]. These findings inspired the development of next generation of gold complexes for the treatment of cancer diseases [11].

Drug repurposing is a strategy that allows existing and approved drugs in clinical settings to be used for other treatment options [12,13]. This constitutes a short cut way to assess drugs conventionally used in other clinical diseases and a fresh approach with the development of resistance to the common drugs. AF besides its anticancer properties shows effective antimicrobial activity against a broad spectrum of bacteria, fungi and parasites [13–18]. Also, CP and analogues were shown to have significant activity as antimalarial and antitrypanosomal agents [19,20].

Based on the similarities between cancer and parasites, recent studies have been run aiming to investigate the effectiveness of existing antiparasitic drugs to treat cancer and the other way round [21]. Moreover, infections are estimated to be responsible for up to 25 % to 50 % of all cancers that occur in humans. Similar to other pathogenic microbes, parasites also elicit chronic inflammation that can induce cancer formation [22,23].

Considering this, it is crucial to understand the mechanisms that are involved in the dual action of anticancer and antiparasitic drugs that can be related to similar target molecules. Among them, a considerable attention has been paid to those involving the inhibition of vital enzymes (oxidoreductases), oxidative stress, and cell death by apoptosis and cell membrane disruption. Thioredoxin reductase (TrxR) is an important and ubiquitous enzyme critically involved in the regulation of intracellular metabolism and in redox signalling. The inhibition of TrxR lead to an increase of the ROS and consequently cell death via apoptosis [24-26]. The thiol-based redox metabolism of trypanosomatids relies exclusively on trypanothione as they lack the canonical redox systems dependent on thioredoxin reductase and glutathione reductase found in most living organisms. Similar to the role of glutathione in mammals, trypanothione provides reducing power for antioxidant defense and other relevant biochemical processes in trypanosomatids [27]. Experimental evidence has shown that even partial inhibition of trypanothione biosynthesis reduces the survival of the parasites in in vivo models and increases their susceptibility to drugs [28-31].

NFX, the reference anti-protozoan drug is metabolized and activated by oxidoreductases to produce free radical species. Under hypoxic conditions, NFX inhibits the survival of cancer cells, although the mechanisms of cytotoxicity need to be further explored [27].

The interest in gold(III) complexes has been inspired from the anticancer properties of CP that shares similar chemical properties and preferential square-planar coordination geometries. Notwithstanding the great attention received, efforts have been focused on the stabilisation of these complexes by selecting less labile ligands, such as *N*-donor and cyclometalated (*C^N*, *C^N^N*) ligands. Sulphur-containing ligands are often introduced to improve the stability of gold(III) complexes, with dithiocarbamates garnered considerable attention [11].

Considering the results obtained previously by some of us [32–35], exploring a series of gold(III) bis(dithiolene) complexes as prospective anticancer, antibacterial and antiplasmodial drugs, herein we selected a lead gold(III) complex and evaluate a class of analogues varying the metal center and the bulkiness of the alkyl chain. In this study, we investigated monoanionic metal bis(dithiolene) complexes, containing N-alkyl-1,3-thiazoline-2-thione dithiolene ligands (R-thiazdt) with alkyl groups exhibiting different steric hindrance (R = Et, tBu), namely [PPh_4] [M(R-thiazdt)₂] with $M^{n+} = Au^{3+}$, Pt^{2+} , Pd^{2+} , Ni^{2+} , called [P][MR] in

this paper for an easier reading (Chart 1). The complexes were assessed towards A2780 and A2780cisR, CP sensitive and CP resistant ovarian cancer cells, respectively and normal cells (HDF and VERO) to evaluate specificity. To overcome the scarcity of compounds targeting trypanosomatid parasites we also screened our complexes against the infective form of *Trypanosoma cruzi* (*T. cruzi*) [36]. The effect of alterations of the ligand skeleton and the transition metal center on the biological properties of theses complexes was evaluated and discussed.

2. Materials and methods

2.1. General methods for chemistry

All reagents and materials from commercial sources were used without further purification. Mass spectra were recorded with a Thermo-Fisher Q-Exactive instrument by the Center Régional de Mesures Physiques de l'Ouest, Rennes. Cyclic voltammograms (CVs) were carried out on a 10^{-3} M solution of complex in $\mathrm{CH_2Cl_2}$ -[Bu₄N][PF₆] 0.1 M solution. CVs were recorded on a Biologic SP-50 instruments at 0.1 V.s⁻¹ on a platinum disk electrode. Potentials were measured *versus* Saturated Calomel Electrode (SCE). The solvents were purified and dried by standard methods. The *N*-Et [37] and the *N*-tBu [38] proligands as well as the [P][NiEt] [39], [P][AuEt] [34], [P][NitBu] [40] and [P][AutBu] [41] complexes were synthesized according to previously reported procedures.

2.2. General synthetic procedures for the synthesis of monoanionic metal bis(dithiolene) complexes from N-Et proligand

To a dry two-neck flask containing the $\it N$ -Et proligand (0.47 mmol, 150 mg) a solution of sodium methanolate in MeOH (Na 43 mg, 1.87 mmol in 20 mL MeOH) was added under argon atmosphere at room temperature. After complete dissolution, the solution was stirred for 30 min at room temperature. Then a solution of Na₂PdCl₄·3H₂O (81 mg, 0.23 mmol) in MeOH (5 mL) or a solution of K₂PtCl₄ (97 mg, 0.23 mmol) in water (5 mL) was added, followed 6 h later by the addition of PPh₄Br (210 mg, 0.50 mmol) in 5 mL of methanol. After stirring for 15 h, the formed precipitate was filtered, washed with MeOH and recrystallized from CH₃CN.

[P] [PdEt] , $C_{34}H_{30}N_2PPdS_8$; Yield: 21 %; mp = 220 °C (dec); HRMS (ESI) calcd for [A $^-$] for [$C_{10}H_{10}N_2S_8^{106}Pd$] $^-$: 519.765 Found: 519.7650; Anal. calcd for $C_{34}H_{30}N_2PPdS_8.CH_3CN$: C, 47.96; H, 3.69; N, 4.66. Found: C, 48.41; H, 3.21; N, 4.97.

[P] [PtEt] , $C_{34}H_{30}N_2PPtS_8$; Yield: 35 %; mp = 190 °C (dec); HRMS (ESI) calcd for [A $^-$] ($C_{10}H_{10}N_2S_8^{195}Pt$): 608.82631 Found: 608.8262; Anal. calcd for $C_{34}H_{30}N_2PPtS_8.CH_3OH$: C, 42.84; H, 3.49; N, 2.86.

Chart 1. Molecular structure of the reference drugs cisplatin, auranofin and nifurtimox and the monoanionic bis(dithiolene) transition metal complexes [P] [MR] investigated in this study.

Found: C, 42.33; H, 3.55; N, 2.72.

2.3. General synthetic procedures for the synthesis of monoanionic metal bis(dithiolene) complexes from N-tBu proligand

To a dry two-neck flask containing the N-tBu proligand (300 mg, 1.14 mmol), a solution of NaOMe (Na: 80 mg, 3.47 mmol) in MeOH (20 mL) was added under argon atmosphere. After complete dissolution, the solution was stirred for 30 min at room temperature. Then a solution of Na₂PdCl₄·3H₂O (200 mg, 0.57 mmol) in MeOH (10 mL) or a solution of K₂PtCl₄ (240 mg, 0.57 mmol) in water (10 mL) was added, followed 6 h later by the addition of PPh₄Br (240 mg, 0.57 mmol) in 5 mL of methanol. After stirring for 15 h, the dark precipitate was filtered and recrystallized from acetonitrile/toluene to afford the monoanionic complexes.

[P] [PttBu], $C_{38}H_{38}N_2PPtS_8$; dark red crystals; Yield: 62 %; mp = 158 °C (dec); HRMS (ESI) calcd for [A $^-$] ($C_{14}H_{18}N_2S_8^{195}Pt$): 664.88891 Found: 664.8891. Anal. calcd for $C_{38}H_{38}N_2PPtS_8$.0.5 toluene: C, 47.41; H, 4.03; N, 2.66. Found: C, 47.07; H, 3.88; N, 2.59.

[P] [PdtBu], $C_{38}H_{38}N_2PPdS_8$; Yield: 26 %; mp = 180 °C (dec); HRMS (ESI) calcd for [A $^-$] ($C_{14}H_{18}N_2S_8Pd$): 575.8276 Found: 575.8279. Anal. calcd for $C_{38}H_{38}N_2PPdS_8$: C, 49.79; H, 4.18; N, 3.06. Found: C, 49.77; H, 3.94; N, 2.53.

2.4. Crystallography

Data collections were performed on an APEXII Bruker-AXS diffractometer equipped with a CCD camera. The structures were solved by direct methods using the SIR92 program [42] and then refined with full-matrix least-square methods based on F^2 (SHELXL-97) [43] with the aid of the WINGX program [44]. All non-hydrogen atoms were refined with anisotropic atomic displacement parameters. H atoms were finally included in their calculated positions. Details of the final refinements are summarized in Table S1 in supporting information. X-ray crystallographic file has been deposited at the Cambridge Crystallographic Data Centre (CCDC 2359353).

2.5. Biological studies

The biological studies were performed by first solubilizing the complexes in DMSO, so in order to evaluate the stability of these complexes in solution of this polar aprotic solvent, we performed ¹H NMR studies for the monoanionic gold complexes (Fig. S1 [45] and a series of UV–vis spectra up to 72 h for the monoanionic radical complexes (Figs. S2, S3 and S4). Analysis of the ¹H NMR and UV–vis spectra shows that over time, these complexes are stable in DMSO solution as no evolution of the spectra is observed.

2.5.1. Cytotoxic activity against ovarian cancer and normal cells

The cytotoxic activity of the complexes was evaluated in A2780 (CP sensitive) and A2780cisR (CP resistant) ovarian cancer cells (Sigma-Aldrich), and in HDF human dermal fibroblasts (Sigma Aldrich) and VERO cells (ATCC CCL81) as normal cell models to test unspecific cytotoxicity. Cancer cells and VERO cells were grown in RPMI-1640 medium (Gibco, Thermo Fisher) supplemented with 10 % fetal bovine serum (FBS) and the normal fibroblasts were grown in Fibroblast Growth Medium (Sigma-Aldrich). All cell lines were maintained at 37 °C, 5 % CO₂ in a humidified atmosphere. For the assays, cells were seeded in 96-well plates at a density of 2×10^4 cells (cancer cells), 1×10^4 10^4 cells (HDF) and 1×10^3 cells (VERO) in 200 μL medium and allowed to attach for 24 h. The bis(dithiolene) complexes were initially dissolved in DMSO and then in culture medium to prepare serial dilutions in the range $0.01-50 \mu M$. The reference compounds were first diluted in saline (CP) or DMSO (AF, NFX) and then in medium in the same concentration range of the dithiolene complexes for CP and AF. For the normal cells, the serial dilutions of NFX were prepared in the range $0.01-100~\mu M$

(HDF) or 0.01–2000 μ M (VERO). After 24 h incubation, the cellular viability was measured by the colorimetric MTT assay, as previously described [32–35]. The percentage of cellular viability was assessed measuring the absorbance at 570 nm using a Power Wave Xs, Bio-Tek plate spectrophotometer for the ovarian cells assays and a Thermo Scientific Varioskan® Flash Multimode spectrophotometer for VERO cells assays. The IC50 values were calculated using the GraphPad Prism software.

For comparison, the CellTiter-Glo assay (Promega) was also used to analyze the number of viable A2780 cells based on the cellular ATP level, which is also a marker for the presence of metabolically active cells. For these assays, A2780 cells were plated in 96-well white opaque plates and then followed the same procedure as above. At the end of 24 h incubation, 100 μL of medium was removed and 40 μL of CellTiter-Glo solution was added in each well. The contents were mixed for 10 min on a shaker and the luminescence recorded using a Varioskan LUX scanning multimode reader (Thermo Fisher Scientific). The percentages of cellular viability in the presence of serial dilution of the complexes were calculated and the IC50 values were determined by the same procedure as the MTT assay.

2.5.2. In vitro activity against trypomastigotes of Trypanosoma cruzi

To establish *T. cruzi's* infections, epimastigotes were stand until a high proportion of metacyclic trypomastigote parasites were observed (~ 7 –8 days). Trypomastigote-rich cultures were incubated overnight with a monolayer of VERO cells in a 10:1 parasite: cell ratio in RPMI medium at 37 °C in a humidified 5 % $\rm CO_2$ incubator. Extracellular parasites were removed the following day by aspirating cell culture media, washing the VERO cell monolayer three times with PBS, followed by addition of fresh complete RPMI. Trypomastigotes emerged from VERO cells (4–5 days) were used to set up new VERO cell infections [46–50]. Cell-derived trypomastigotes to use in testing experiments were obtained from the supernatant of infected VERO cells collected 72 h post established infection with cell-emerged trypomastigotes [46–50].

For the assays, the compounds were initially dissolved in DMSO at $11.25 \,\mu\text{M}$ (stock concentration). The solution was diluted in the culture medium to obtain the different concentrations tested. Throughout the experimental procedures, the concentration of DMSO never exceeded 1 %, which is non-toxic for the protozoa [51].

Parasites were seeded in black 96 well plates in RPMI at a density of 1×10^7 parasites/mL with increasing concentration of the compound for 24 h. Viability was tested using the Alamar Blue (resazurin) assay, which is based on the reduction of resazurin to highly fluorescent resorufin in the presence of metabolically active cells. For the assays, 50 μL of resazurin solution (2 mg/mL in RPMI) were added to each well and incubated for 4 h at 28 °C or 37 °C. Fluorescence ($\lambda_{ex}=530$ nm/ $\lambda_{em}=590$ nm) was measured in a Thermo Scientific Varioskan® Flash Multimode plate spectrofluorimeter instrument [46–51]. NFX was used as the reference anti-T. cruzi drug. Dose-response curves were built and the IC50 values were determined using GraphPad Prism version 8.00. The results are presented as mean \pm SD of three independent biological replicates.

2.6. Apoptosis (caspase 3/7)

Caspase-3 and -7 activities were assessed using a Caspase-Glo®3/7 luminescent assay (Promega). The assay provides a proluminescent caspase-3/7 substrate, with proluciferin DEVD substrate. This substract is cleaved in the presence of caspase 3/7 to release the aminoluciferin used in the production of light. The luminescent signal is proportional to the caspase activity present in the cells. The assays were carried out with the A2780 cells in white-walled 96 well plates, treated with the complexes at concentrations below the IC50 values for 24 h. After incubation, 100 μL of medium was removed from each well. Caspase 3/7® reagent was added in a 1:1 ratio and the plate was shaken in an orbital shaker for 30s at 300 rpm. The plate was incubated at room temperature for 1.5 h,

protected from light. The luminescence intensity was measured using a Varioskan LUX scanning multimode reader (Thermo Fisher Scientific). Results (mean \pm SD) were expressed as the fold change in luminescence compared with controls (non-treated cells).

2.7. Apoptosis (SEM)

For the SEM studies, A2780 cells were seeded over glass lamellae in 6-well plates at a density of 2×10^5 cells in 2 mL medium and allowed to attach for 24 h. After, the complexes [P][PttBu] and [P][PdtBu] were added to the cells in culture medium at a concentration corresponding to their IC_{50} values, 4 μM and 1 μM , respectively. After 24 h incubation, the medium was discarded and the cell-covered glass lamellae were fixed in 2 mL of 3 % glutaraldehyde in 0.1 M sodium cacodylate buffer, pH 7.3 for 4 h at 4 °C and rinsed three times in the same buffer. The lamellae were then dehydrated in ascending ethanol concentrations and treated three times with tert-butanol. After cooling at 4 $^{\circ}\text{C}$ in a refrigerator, the solid samples were transferred to a vacuum desiccator containing a cooled metal block to prevent the liquefaction of the cold tert-butanol. The desiccator was evacuated using a rotary vacuum pump for two hours to allow complete sublimation of the solid tert-butanol. The freeze-dried samples were coated with gold in a JEE-4× vacuum evaporator and observed and photographed using a JEOL 5400 scanning electron microscope.

2.8. Intracellular ROS

2.8.1. Detection of ROS by H2DCF-DA

Detection of ROS, mainly peroxides were measured using the 2',7'dichlorodihydrofluorescein diacetate (H2DCF-DA) fluorescent probe as previously described [32]. H₂DCF-DA enters into the cells, where it is oxidized to fluorescent DCF by the action of intracellular stearases. It is generally assumed that DCF-based probes are relatively specific detectors of H_2O_2 . For the assays, A2780 cells (~10⁴ cells/well) were seeded in black-walled 96 well plates and left to adhere overnight. Then, the medium was replaced with 200 μL solution of the probe at 10 μM in colorless DMEM medium (FluoroBrite™ DMEM, Gibco) and incubated with the cells for 20 min. at 37 °C. After, the probe was removed and replaced by fresh medium with the bis(ditholate) complexes and the reference drugs CP and AF at 10, 20, 50 and 100 μM for 1 h. DCF fluorescence ($\lambda_{ex} = 485$ nm; $\lambda_{em} = 530$ nm) was measured using a Varioskan LUX scanning multimode reader (Thermo Fisher Scientific). Results (mean \pm SD) were expressed as the fold change in fluorescence levels compared with controls (non-treated cells).

2.8.2. Detection of superoxide radicals (NBT assay)

The nitro blue tetrazolium (NBT) assay was carried out adapting previously described methods [32,52,53]. This assay is based on the reduction of NBT by superoxide anion upon treatment with the complexes, resulting in the formation of dark-blue formazan particles. Briefly, after incubation of A2780 cells with the complexes in medium at selected concentrations for 1 h at 37 °C, 20 μL of a 10 mg/mL NBT solution in water was added to the cell's medium, and incubation was subsequently prolonged for 1 h at 37 °C. Then, the medium was discarded, and the dark-blue formazan particles formed upon NBT reduction were dissolved with 200 μL of a solution containing 90 % DMSO:10 % NaOH 0.1 N with 0.1 % SDS. The resulting NBT formazan was measured at 560 nm using a plate spectrophotometer.

2.9. Detection of lipid droplets

The Nile Red (phenoxazine dye) (Sigma-Aldrich) is a lipophilic fluorescent dye that has the ability to stain and visualize lipid droplets in cells and tissues [54]. First, a stock solution of 3 mM in DMSO was prepare and then 1:300 dilution in colorless medium (FluoroBriteTM DMEM, Gibco) was made for the cells. For the assays, A2780 cells (2 \times

 10^4 cells/well) were seeded in black-walled 96 well plates and left to adhere overnight. After 1 h treatment with the complexes, the cell media was aspirated and an equal volume (200 $\mu L)$ of Nile Red staining solution in FluoroBrite^TM DMEM was added, followed by incubation at 37 °C, 5 % CO2 for 30 min. The Nile Red was removed and fluorescence was measured at $\lambda_x/\lambda_m=550/640$ nm using a plate spectrofluorimeter instrument.

3. Results and discussion

3.1. Synthesis and redox properties of the metal bis(dithiolene) complexes

The monoanionic palladium and platinum bis(dithiolene) complexes were prepared from the N-Et and the N-fBu proligands, according to the synthetic strategy previously used for the synthesis of the analogous monoanionic gold and nickel complexes [38–41], (Scheme 1). Even if the dithiolene proligands are different, as for the N-Et proligand the dithiolene is protected by two cyanoethyl groups while for the N-fBu the dithiolene ligand is inserted in a dithiol-2-one heterocycle, the deprotection step is the same. The chemical approach consists of, first the deprotection of the dithiolene ligand, by adding a solution of sodium methanolate, NaOMe, followed by the subsequent addition of the appropriate metallic salt (NiCl₂-6H₂O, K_2 PtCl₄, Na_2 PdCl₄ or $KAuCl_4$) and Ph_4PBr to afford the monoanionic metal complexes. The eight metal bis(dithiolene) complexes prepared and investigated in this study are collected in Chart 1.

Crystals of [P][PttBu] were obtained, and the molecular structure is presented in Fig. 1. The [P][NitBu] and [P][PttBu] complexes crystallize as a toluene solvate when recrystallized from an acetonitrile/toluene solution, and [P][NitBu] as a non-solvate when recrystallized from $CH_2Cl_2/MeOH$. The three crystal structures are solved in the monoclinic system, space group C2/c. The non-solvated [P][NitBu] [40] crystal is isostructural with the [P][AutBu] [41], while the [P][NitBu] [40] toluene solvate is isostructural with the [P][PttBu].

For both [P][NitBu] complexes (in non-solvated and solvated forms) and the [P][PttBu] complex, the metallic atom is on an inversion center, and phosphorous atom is on a two-fold axis. For the solvated complexes the toluene molecule is disordered on two positions related by an inversion center. The complexes are almost completely planar, with a dihedral angle $\Theta_{S \bullet \bullet \bullet S}$ of 4.1° within the metallacycle for the non-solvated and 0.8° (Ni) 0.5° (Pt) for the solvated ones. The ligands adopt the *trans* configuration around the metal atom in all the cases, which is similar to what is seen for the gold analogue, [P][AutBu] [41]. The comparison of the bond distances collected in Table 1 shows that the tBu group or the Et one on the nitrogen atoms, does not have a significant effect on the bond lengths of the metallacycle, or those of the thiazole ring. On the other hand, the change of the metal atom from gold to nickel or platinum decreases the C—S bonds of the metallacycle as expected.

The redox properties of the different complexes were studied by cyclic voltammetry. Indeed, dithiolene ligands are non-innocent ligands and thanks to electron delocalization over the metallacycle, generated by the mixing of the metal and ligand orbitals, these complexes present several redox states [55]. This study was performed in a dichloromethane solution with [Bu₄N][PF₆] 0.1 M as a supporting electrolyte, at a scan rate of $100 \, \text{mV.s}^{-1}$ using a platinum working electrode. The redox potentials were measured in V vs. SCE (saturated calomel electrode) and the data are collected in Table 2. The nickel, palladium, and platinum bis (dithiolene) complexes can exist under four redox states (Scheme 2), and on the cyclic voltammograms, three redox processes can be observed (Fig. 2).

The first two correspond to the successive oxidation of the dianion into the monoanion radical at $E_1(-2/-1)$ and of the monoanion into the neutral species at $E_2(-1/0)$. These two redox waves were already reported by Arca et al. when they analyzed the redox activity of the corresponding neutral complexes [MEt] (M = Ni²⁺, Pd²⁺, Pt²⁺) [56,57].

Scheme 1. Synthetic path to the monoanionic metal bis(dithiolene) complexes.

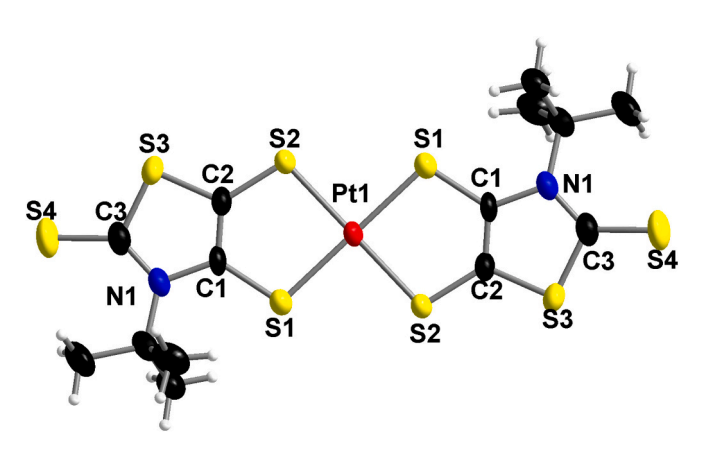


Fig. 1. Molecular view of the monoanionic complex [PttBu]⁻ with thermal ellipsoids at the 80 % probability level.

The last oxidation process, unlike the other two, is quasi reversible and corresponds to the oxidation of the neutral species to the monocation $E_3(0/+1)$.

As expected, changing the alkyl substituent on the nitrogen atom of the thiazoline ring, Et for *t*Bu, does not significantly modify the redox potentials of the different complexes studied (Table 2). However, for a given metal all the *N-t*Bu complexes are easier to oxidize than their corresponding *N*-Et ones. Regarding the gold complexes, they also can exist under four redox states but this time the radical state is the neutral one while for the Ni, Pt and Pd complexes the radical state is the monoanionic one. The monoanionic gold complexes are more difficult to oxidize to the neutral state than all the other reported complexes.

The UV–vis-NIR spectroscopic investigations were carried out for all the synthetized complexes on freshly prepared dichloromethane solutions (10^{-5} M) of the monoanion. The absorption maxima (λ_{max}) of the NIR absorption bands are collected in Table 2. All the Ni, Pt and Pd complexes exhibit absorption band in the NIR region while the Au

Table 2 Wavelength of the lowest energy absorption band λ_{max} (nm) and redox potentials of the complexes [P][MR] in CH₂Cl₂ with [Bu₄N][PF₆] 0.1 M, E in V vs. SCE, scan rate of 100 mV·s⁻¹.

[P][MR]	$\lambda_{\text{max}}(\text{nm})$	$E_{pa}/E_{pc}^{1}(-2/-1)$	$E_{pa}/E_{pc}^2(-1/0)$	$E_{pa}/E_{pc}^{3}(0/+1)$
[P][NiEt]	1280	-0.30/-0.36	0.23/0.17	1.08/0.99
[P][PdEt]	1560	-0.15/-0.20	0.26/0.20	1.08/1.02
[P][PtEt]	1260	-0.28/-0.35	0.24/0.16	1.07/0.93
[P][AuEt]	364	-/-0.90	0.55/0.49	0.71/0.61
[P][NitBu]	1228	-0.40/-0.46	0.16/0.10	0.93/0.82
[P][PdtBu]	1532	-0.23/-0.29	0.20/0.13	0.91/-
[P][PttBu]	1232	-0.37/-0.43	0.17/0.09	_
[P][AutBu]	374	-/-1.08	0.48/0.44	0.57/-

complexes exhibit the lowest energy absorption band in the UV-vis region only.

Similar trends are observed for all studied metal bis(dithiolene) complexes as illustrated in Fig. 3, showing the absorption spectra of [P] [MEt] with $M^{2+}=Ni^{2+},\,Pd^{2+}$ and $Pd^{2+}.$ These monoanionic species exhibit a strong absorption band in the NIR region. The NIR region 1680–1720 nm of the [P][PdEt] spectrum has been omitted due to absorption bands of dichloromethane associated with overtones and combination peaks involving C—H stretch vibrations. The nature of the metal ion induces some differences on the absorption spectra, especially on the wavelength of the lowest energy absorption band. For instance, if we consider the monoanionic complexes with the same ligand, the λ_{max} of the NIR absorption band for the Pd complex is significantly redshifted ($\approx\!300$ nm) compared to that of its Ni and Pt analogues. The Ni and Pt present relatively close λ_{max} for the lowest energy band. This is in line with what was observed upon electrochemical investigations.

3.2. In vitro activity against ovarian cancer cells

Ovarian cancer is the third most common female cancer in the world. High-grade serous is the most prevalent type of ovarian cancer, accounting for 70 % of deaths. Although significant advances have been

Table 1Bond distances (Å) of the ligands in the [P][MR] complexes.

S O S O D S O D D S O D D S O D D D D D	[P][NiEt] [39]	[P][NitBu] [40]	Toluene [P][NitBu] [40]	Toluene [P][PttBu]	[P][AutBu] [41]
a	2.156(1)	2.149(1)	2.153(1)	2.2728(9)	2.327(1)
a'	2.178(2)	2.172(3)	2.162(1)	2.2776(7)	2.310(1)
b	1.712(3)	1.717(6)	1.715(4)	1.708(3)	1.767(5)
b'	1.722(2)	1.733(5)	1.732(4)	1.728(3)	1.740(5)
c	1.356(3)	1.362(7)	1.357(5)	1.367(5)	1.349(6)
d	1.739(2)	1.735(4)	1.725(4)	1.738(4)	1.724(5)
e	1.735(3)	1.731(14)	1.732(4)	1.733(4)	1.735(6)
f	1.664(3)	_	1.671(4)	1.677(3)	1.679(7)
g	1.362(4)	1.398(8)	1.367(5)	1.373(5)	1.374(8)
h	1.398(3)	1.440(8)	1.422(4)	1.427(4)	1.430(7)
$\Theta_{S \bullet \bullet \bullet S}$	10.91	4.12	0.87	0.50	7.75

Scheme 2. Representation of the four redox states of metal bis(dithiolene) complexes.

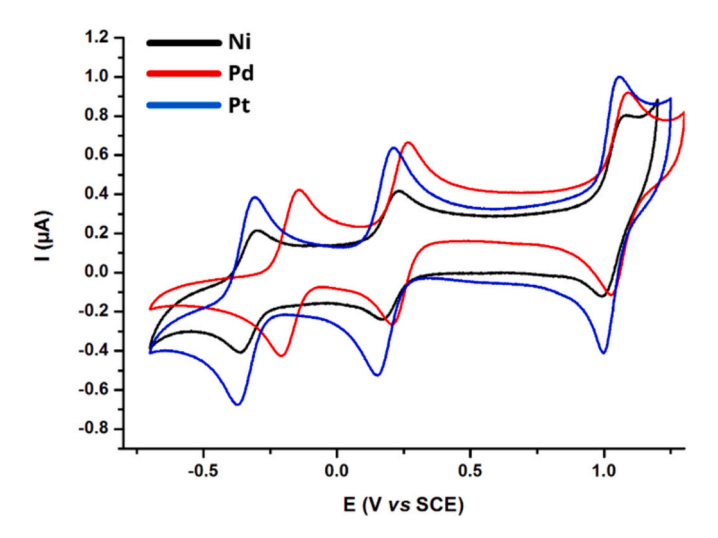


Fig. 2. Cyclic voltamograms of [P][MEt] $M^{2+}=Ni^{2+}$, Pd^{2+} , Pt^{2+} in CH_2Cl_2 with [NBu₄][PF₆] 0.1 M, E in V ν s. SCE, scan rate of 100 mV.s⁻¹.

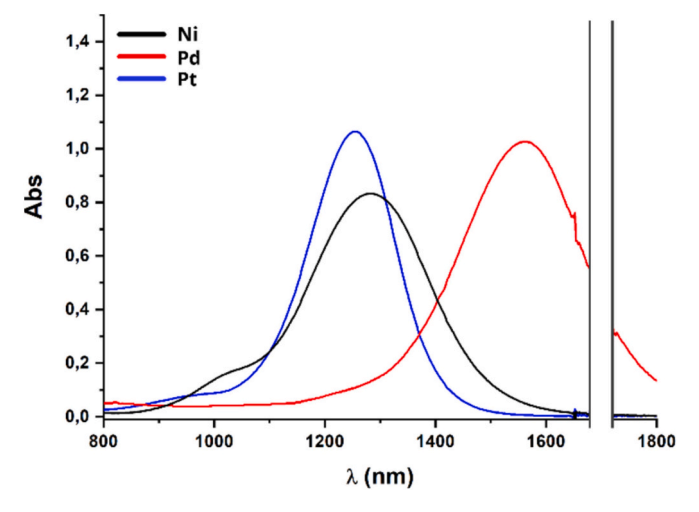


Fig. 3. NIR absorption spectra of [P][MEt]. $M^{2+} = Ni^{2+}$, Pd^{2+} , Pt^{2+} . The absorption between 1650 and 1750 nm was removed due to the presence of an artifact.

made in the treatment of this type of cancer, recurrence is observed up to 80 % at advanced stages [58,59]. Currently, the basic treatment of ovarian cancer is surgery combined with chemotherapy and/or radiotherapy. CP and analogues are the standard treatment, despite their

severe side effects and development of resistance [60]. Several drugs are currently undergoing repurposing against ovarian cancer, including AF. The mechanism of action shared for both CP and AF include induction of oxidative stress characterized by ROS accumulation, cell cycle arrest and activation of apoptosis [3,60,61]. AF has been studied exploring the cytotoxic effect in ovarian cancer. However, few studies have been done with the AF-sensitive A2780 ovarian cancer cells that represent the high-grade serous histotype [62].

Drug discovery and development often include cytotoxicity testing. These assays are useful to evaluate enzymatic activity or general metabolism, with methods often utilising absorbance or luminescence detection. The cytotoxic activity (IC_{50} values) of the complexes was evaluated using the MTT and ATP assays. MTT is reduced by mitochondrial dehydrogenases in living cells to a purple formazan product. The absorption of formazan in the visible region correlates with the number of intact alive cells. ATP is formed exclusively in the mitochondria that represents the most important chemical energy reservoir in cells necessary for biological processes. When cells lose membrane integrity, they lose the ability to synthesize ATP and endogenous ATPases rapidly deplete any remaining ATP from the cytoplasm. The best method to measure intracellular ATP is using the firefly luciferase which catalyses the oxidation of D-luciferin to oxyluciferin [63].

In our study, the anticancer activity of the eight-metal based bis (dithiolene) complexes by the MTT assay was evaluated in the A2780 and A2780cisR ovarian cancer cells after exposure to increasing concentrations of the complexes (0.01–50 $\mu M)$ for 24 h, at 37 $^{\circ} C$, 5 % CO₂ (Table 3, Fig. S5). The A2780cisR cells were included to evaluate the ability of the complexes to overcome CP resistance.

Results showed that all the complexes displayed high cytotoxic activities even at short incubation times (24 h) similar to AF with IC $_{50}$ values ranging from 0.6 to 4 μM (A2780) and 1–7 μM (A2780cisR). All the complexes presented higher activities compared to CP, and most importantly, were active against the A2780cisR cells. Interestingly, the nature of the alkyl substituent on the thiazole ring modifies their activity, since the *N*-Et substituted complexes with the same metal are more cytotoxic than the *N*-tBu ones on both ovarian cancer cells. The reference antiparasitic agent NFX (0.01–100 μM) was also included in the study and showed no cytotoxic activity against both cell lines (IC $_{50}$ > 100 μM).

The selectivity index (SI) was calculated from the IC_{50} values of normal cells (HDF) vs. A2780 cells and indicated for the majority of the complexes good anticancer specificity (SI > 3) with clinical relevance for [P][PdtBu] (SI = 10). [64]

The cellular viability based on detection of ATP release was also evaluated by a luminescence assay in the A2780 ovarian cancer cells (Table 4, Fig. S7). Cells were exposed to increasing concentrations of the complexes and the reference drugs AF (0.01–50 μ M) and CP (0.1–100 μ M) for 24 h, at 37 °C. Results show that all complexes displayed lower

Table 3 IC_{50} values (μ M) calculated for the Au, Pt, Pd and Ni bis(dithiolene) complexes and the reference drugs CP, AF and NFX with the ovarian cancer cells and the human dermal fibroblasts (HDF) after 24 h treatment using the MTT assay. Results are the mean \pm SD of three independent experiments done with six replicates.

Complex	HDF IC ₅₀ (μM), 24 h	A2780 IC ₅₀ (μM), 24 h	A2780cisR IC ₅₀ (μΜ), 24 h	SI HDF/A2780 cells
[P][AuEt]	3.98 ± 0.66	0.70 ± 0.24	1.09 ± 0.36	5.68
[P][PtEt]	5.62 ± 1.50	1.76 ± 0.62	3.64 ± 0.95	3.19
[P][PdEt]	2.63 ± 0.73	1.27 ± 0.39	0.81 ± 0.39	2.07
[P][NiEt]	2.29 ± 0.62	1.21 ± 0.45	2.04 ± 0.56	1.89
[P][AutBu]	6.93 ± 1.27	1.47 ± 0.42	7.32 ± 1.48	4.71
[P][PttBu]	15.4 ± 4.22	4.20 ± 0.87	9.23 ± 1.22	3.67
[P][PdtBu]	9.68 ± 2.80	0.97 ± 0.36	6.70 ± 1.51	9.97
[P][NitBu]	7.78 ± 1.55	2.10 ± 0.70	5.51 ± 0.64	3.70
CP	13.8 ± 5.66	18.9 ± 2.07	31.6 ± 7.10	0.73
AF	0.16 ± 0.04	2.50 ± 1.06	1.96 ± 0.67	0.06
NFX	82.5 ± 21.8	$> 100~(159 \pm 13.5)$	>100	< 0.83

SI refers to Selectivity Index, SI value >3 indicating good selectivity.

cytotoxicity compared to the MTT assay with IC_{50} values ranging from 3.5 to 9.5 μ M (A2780) but following the same trend that indicated [P] [PttBu] to be the less active complex in the ovarian cancer cells.

3.3. In vitro activity against T. cruzi and selectivity towards the parasites

The main problems with current drugs for the treatment of protozoan infections caused by trypanosomatid parasites are their severe side effects due to the prolonged treatment regimens and the emergence of resistance. New improved treatment options and new drugs are urgently needed [65]. To circumvent the difficulties associated with the development of novel antiparasitic drugs that are, among others, poor investment on tropical diseases research by pharmaceutical companies, one alternative is to focus on existing drugs being used to treat other human diseases and test them for their antiparasitic properties. The diversity of prospective drugs as anticancer agents and the available data relative to their pharmacology and toxicity are essential factors that ultimately influence the overall costs in the development of drugs for parasitic diseases. As there are a number of crucial links between cancer cells and parasites, it has been observed that a number of antitumor agents have shown antitrypanosomal effects and conversely, several antitrypanosomal compounds demonstrated activity against cancer diseases [66].

Chemotherapy is still the most cost-effective treatment of tripanosomatid diseases. NFX, a nitrofurane derivative has been used against *Trypanosoma cruzi*, the agent of Chagas' disease, commonly known as American Trypanosomiasis. Therapy with NFX is prolonged and severe side effects are common, including gastrointestinal, neurological and hematological effects. One of the modes of action of NFX proposed, involves the reduction by parasite enzymes of the nitro-group to a nitro-

Table 4 IC $_{50}$ values (μ M) calculated for the Au, Pt, Pd and Ni bis (dithiolene) complexes with the ovarian cancer cells (A2780) after 24 h treatment using the ATP assay. Results are the mean \pm SD of three independent experiments done with four replicates.

Complex	A2780 IC ₅₀ (μM), 24 h
[P][AuEt]	5.65 ± 1.02
[P][PtEt]	7.62 ± 1.00
[P][PdEt]	5.03 ± 0.66
[P][NiEt]	4.99 ± 0.41
[P][AutBu]	4.18 ± 0.54
[P][PttBu]	9.86 ± 1.52
[P][PdtBu]	3.42 ± 0.59
[P][NitBu]	3.65 ± 0.60
CP	14.5 ± 2.7
AF	1.20 ± 0.19

anion radical, which undergoes redox-cycling with molecular oxygen, leading to the production of ROS and inhibition of trypanothione reductase a parasite-specific antioxidant [67,68]. In some cases, the concentration of ROS correlated with the antiparasitic activity of the compounds [65].

Medicinal Inorganic Chemistry currently offers an attractive option for the rational design of new antiparasitic drugs. In this direction, a strategy for the design of metal-based antiparasitic compounds has been the coordination of an organic ligand with known biological profile to a metal centre or an organometallic core [69,70]. Moreover, these metal coordination complexes could display multifunctional properties in a single molecule and offer dual action for cancer and microbial infection [32–34].

In our study, the eight metal bis(dithiolene) complexes were evaluated in vitro for their anti-T. cruzi activities against the infective trypomastigote form of the Dm28c clone. The activities expressed by the IC_{50} values were determined by viability assays after parasite incubation with increasing concentrations of the complexes. In parallel, cytotoxicity on VERO cells as a normal mammalian cell model was assessed to evaluate the selectivity towards the parasites. The results were compared to the reference drug NFX (Table 5, Figs. S8 and S9).

All the complexes showed activity against T. cruzi in the micromolar range, in the same order of magnitude compared to NFX when they were exposed for 24 h. Except for [P][PdEt], it was observed that complexes containing the ethyl group exhibited toxicity towards VERO cells, with IC₅₀ values even lower than those determined for parasites. This observation led to the characterization of these complexes as nonselective (SI < 1). In fact, [P][PdEt] also displayed limited selectivity, with an SI value of 2.6. Complexes containing tBu exhibited an enhanced selectivity index (SI > 10), with [P][PttBu] and [P][PdtBu] appearing to be the most selective complexes. Notably, the IC_{50} values (> 50 μM) for these compounds in the VERO cells could not be determined accurately due to absorption interference at 570 nm caused by a slight precipitation of the complexes at high concentrations. The selectivity observed for these two complexes, [P][PttBu] and [P][PdtBu] could be ascribed to the presence of bulkier substituent on the metal bisdithiolene complexes backbone.

3.4. ROS studies

Reactive oxygen species (ROS) are chemically reactive molecules produced by cellular metabolism. At moderate levels they play essential role in the regulation of cell proliferation and cell survival [72]. However, high ROS levels can cause damage to cellular components such as proteins, DNA and lipids. In particular, ROS can disrupt the lipid membrane increasing membrane fluidity and permeability. Several anticancer drugs act by inhibiting and suppressing cancer progression through ROS-mediated cell death [53,73].

ROS are highly reactive and extremely unstable molecules.

Table 5
In vitro activity (IC₅₀) against *T. cruzi* (Dm28c clone) and VERO mammalian cells (VERO cells) calculated for the Au, Pt, Pd and Ni bis(dithiolene) complexes and the reference drug NFX after 24 h treatment using the Alamar Blue assay. Results are the mean \pm SD of three independent biological replicates.

Complex	VERO cells IC ₅₀ (μM)	T. cruzi Trypomastigotes IC ₅₀ (μM)	SI VERO cells/Trypomastigotes
[P][AuEt]	1.10 ± 0.04	3.34 ± 0.37	0.33
[P][PtEt]	2.77 ± 0.60	5.18 ± 0.96	0.53
[P][PdEt]	12.3 ± 1.8	4.63 ± 0.55	2.65
[P][NiEt]	3.2 ± 1.7	5.56 ± 0.67	0.58
[P][AutBu]	24.0 ± 2.2	5.79 ± 0.49	4.14
[P][PttBu]	> 50	4.67 ± 0.61	> 11
[P][PdtBu]	> 50	2.91 ± 0.85	> 17
[P][NitBu]	9.99 ± 0.66	2.60 ± 0.11	3.84
NFX	$998\pm91^{\rm a}$	$3.35\pm0.87^{\mathrm{b}}$	298

SI = Selectivity index calculated for each complex using the formula: $SI = (IC_{50} \text{ for normal cells VERO})/(IC_{50} \text{ for } T. \text{ cruzi trypomastigotes}).$

^b Data obtained under identical assay conditions as Ref 49.

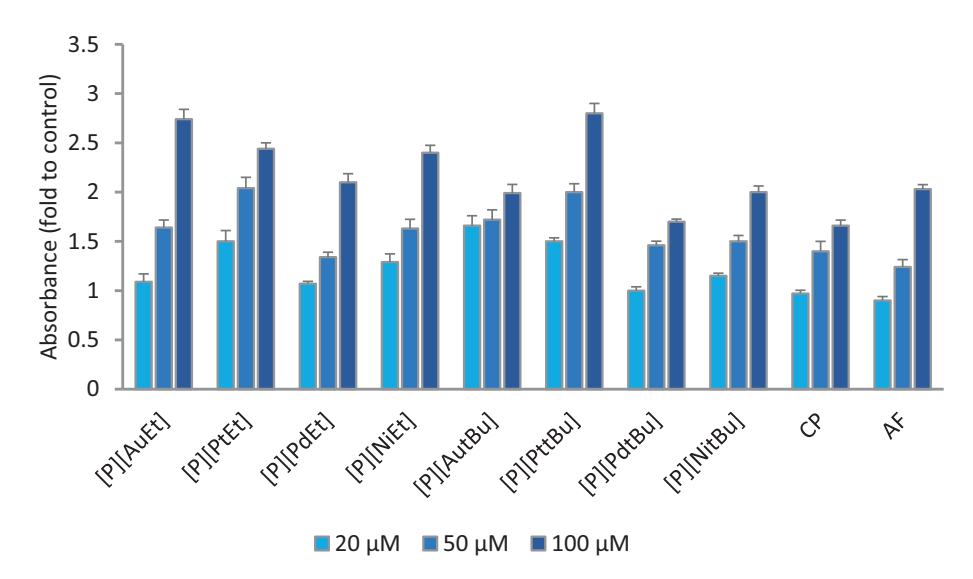


Fig. 4. ROS production (namely H_2O_2 , OH^{\bullet} or $ONOO^{-}$) by the A2780 cells using the H_2DCF -DA method based on the detection of DCF fluorescence. Cells were treated with the complexes at 10, 20, 50 and 100 μ M for 1 h. The reference drugs CP and AF were also included for comparison. Results in fluorescence (fold to control) are mean \pm SD of at least 2 experiments with 3 replicates per condition.

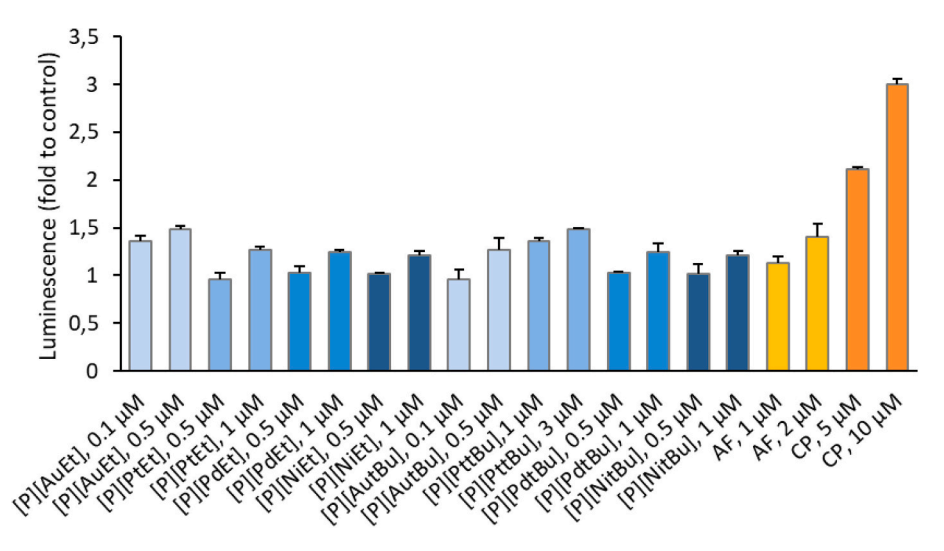


Fig. 5. ROS production (superoxide, $O_2^{\bullet-}$) by the A2780 cells using the NBT absorbance method based on the detection of the blue precipitates of formazan particles. Cells were treated with the complexes at 20, 50 and 100 μ M for 1 h. The reference drugs CP and AF were also included for comparison. Results in absorbance (fold to control) are mean \pm SD of at least 2 experiments with 4 replicates per condition. (For interpretation of the references to colour in this figure legend, the reader is referred to the web version of this article.)

^a Data obtained under identical assay conditions as Ref. 71.

Therefore, their detection relies on the measurement of the end products that are formed when these molecules react with particular agents. The main ROS species include hydrogen peroxide (H_2O_2) , peroxynitrite (ONOO^-) , hydroxyl radical (OH^\bullet) and superoxide (O_2^\bullet) . The induction of intracellular ROS namely H_2O_2 , OH^\bullet or $ONOO^-$ by the complexes in A2780 cells was analyzed using the $H_2\text{DCF-DA}$ fluorescent probe, one of the most widely used methods for directly measuring the redox state of a cell. Therefore, $H_2\text{DCF-DA}$ oxidation should be interpreted as an indication of the general cellular oxidative stress due to action of the complexes.

The effect of the bis(dithiolene) complexes on ROS production by A2780 cells are shown in Fig. 4. Despite most of the complexes exhibited similar cytotoxicity towards the cancer cell under study, their ROS production profiles were distinct. Among these complexes, if we compare, for a given metal, the influence of the alkyl group on the production of ROS, for the tBu substituted complexes at the concentrations 10, 20 and 50 μ M, less reactive oxygen species are generated than with the N-Et substituted complexes. However, this trend is less pronounced for the highest concentration, 100 µM, although it was shown that a slight precipitation occurred for some complexes, namely ([P] [PttBu] and [P][PdtBu]) at high concentrations (> 50 µM). Another interesting feature is that the ROS evolution is also metal dependent in both series. Besides the gold complexes, a clear increase of the ROS production is observed which was dependent on the concentration of the added complex. Despite a similar geometry with these bis(dithiolene) complexes, the main difference relies on their redox properties. All these monoanionic complexes are redox active species, which can be easily oxidized to the neutral species only for the Ni, Pt and Pd complexes compared to the Au complexes. The other difference is that Ni, Pt and Pd complexes have an odd number of total electron and are therefore radical monoanionic species. The reference drugs CP and AF were tested at the same concentrations and showed lower ROS production than the complexes under study.

The ROS species superoxide $(O_2^{\bullet-})$ was detected with the nitro blue tetrazolium (NBT), a cell-permeant nitro-substituted aromatic tetrazolium salt, with the ability to interact with superoxide in the cytoplasm to form dark-blue precipitates of formazan particles [74]. As shown in Fig. 4 and Fig. 5, complexes and the reference drugs, although to a lesser extent, increased the ROS levels in a dose-dependent manner, with ROS production being considerably higher when compared with the controls (untreated cells).

3.5. Caspase studies

3.5.1. Caspase 3/7 activity

Apoptosis is the main mechanism of cancer cell death by chemotherapeutic drugs. The intracellular process is mediated, at least partially, by a series of cysteine proteases, namely caspases. ROS generation often lead to induction of apoptosis through caspase activation [75]. The caspase cascade following cytochrome c release is initiated by caspases-8 and -9 that activate the executioner's caspases-3, -6 and -7, enabling cell death [76]. We explored the use of the active form of caspase-3 and -7 for the detection of apoptotic events induced by the complexes. Complexes were tested at concentrations below their IC50 values at 24 h (Fig. 6). Their ability to activate caspase-3/7 is dosedependent and similar to that of the gold reference AF, but much lower than CP that showed high caspase activation ability, which seemed to be in agreement with other studies that support a model for the CP-sensitive A2780 cells in which cisplatin-induced cell death proceeds via caspase-3-independent pathways, such as by binding to DNA and promoting apoptosis [77-79].

3.5.2. Detection by SEM

The morphological features of cells undergoing apoptosis can be detected through the analysis of scanning electron microscopy (SEM). The cell-surface changes, including membrane blebbing and loss of features, such as microvilli, can be observed by SEM [80]. Fig. 7 shows cells under division (white cells) and cells with surface changes that could indicate membrane blebbing. Nevertheless, cells that probably are undergoing apoptosis are also present in control cells (no treatment). Results seemed to be in agreement with those of caspase 3/7 assays (Fig. 6) that show complexes's low ability to activate caspase.

3.6. Lipid droplets (LDs) study

The increase of intracellular ROS levels can affect the homeostasis of intracellular lipid metabolism, promoting the accumulation of intracellular lipid droplets (LDs), now emerging as major regulators of cellular metabolism. Although this specific regulatory mechanism is not yet clear, previous studies observed enhanced LDs accumulation in cells exposed to oxidative stress. Thus, LDs emerged as dynamic organelles that are essential for the cellular response to metabolic stress. In addition, after induction of apoptosis, accumulation of cytoplasmic LDs can lead to cell death [81,82].

The effect of the dithiolene complexes on LDs formation A2780 cells are shown in Fig. 8. Although preliminary, these studies indicated the

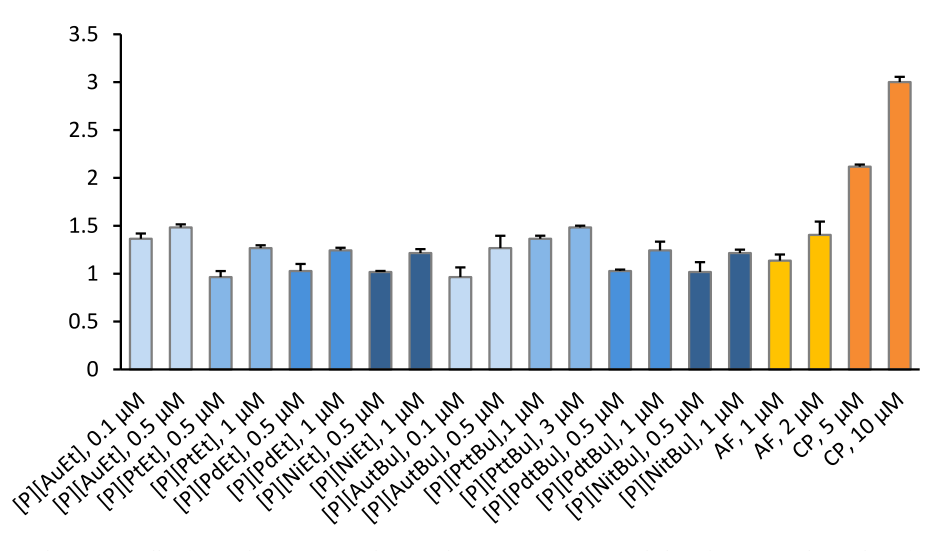


Fig. 6. Caspase 3/7 activity in the A2780 cells after 24 h exposure to the complexes at concentrations below their IC_{50} values. The reference drugs CP and AF were also included for comparison. Results in luminescence (fold to control) are mean \pm SD of at least 2 experiments with 4 replicates per condition.

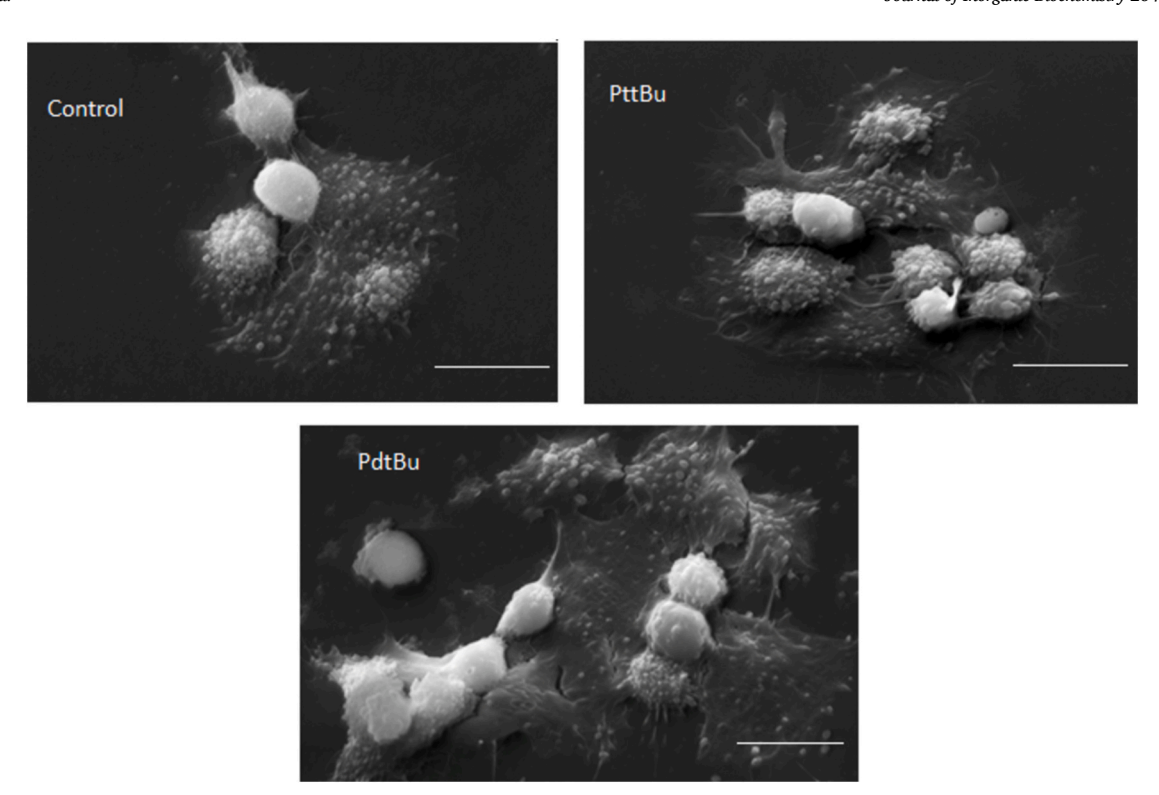


Fig. 7. Scanning electron microscopy (SEM) of A2780 cells: non-treated cells (control) and treated cells with [P][PttBu] and [P][PdtBu] at their IC₅₀ values at 24 h, 4 μ M and 1 μ M respectively. Bars = 20 μ m.

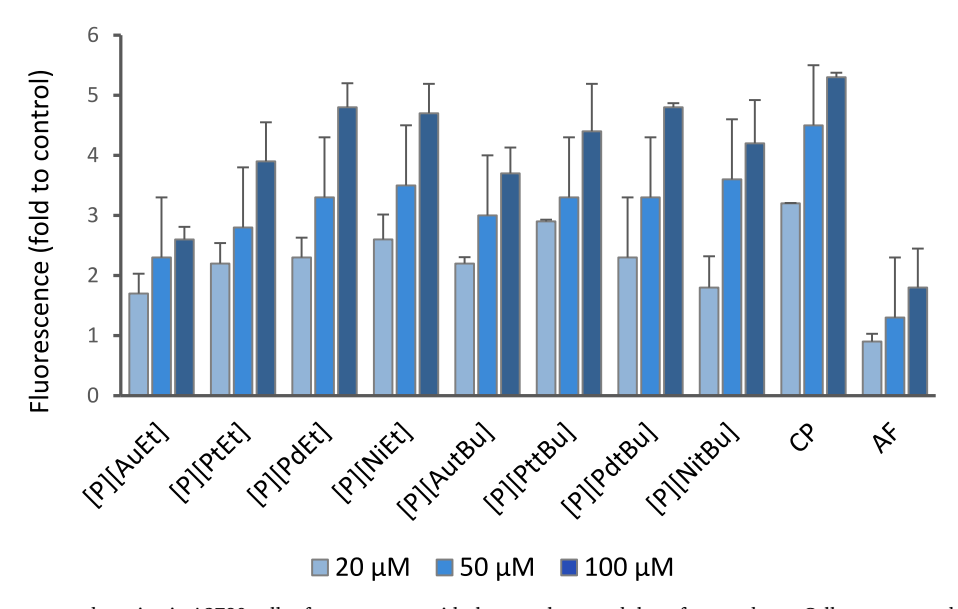


Fig. 8. Lipid droplets fluorescence detection in A2780 cells after treatment with the complexes and the reference drugs. Cells were treated with the complexes at 20, 50 and 100 μ M for 1 h. The reference drugs CP and AF were also included for comparison. Results in fluorescence (fold to control) are mean \pm SD of at least 2 experiments with 4 replicates per condition.

formation of LDs upon treatment with the compounds at 20, 50 and 100 μ M and that this effect is dose-dependent. However, the relationship between ROS generation and the formation of LDs was not evident, except for the [P][PtfBu] complex.

4. Conclusions

In this study we report the synthesis of four new monoanionic metal bis(dithiolene) complexes with Pt and Pd metal centers, coordinated to two 2-thioxo-1,3-thiazoline-4,5-dithiolene ligands substituted by alkyl groups of different bulkiness such as Et and tBu. The electrochemical, structural and optical properties of these complexes were compared with those of their previously reported Au and Ni analogues and no significant effect of the alkyl group was demonstrated. Among these monoanionic complexes, the redox as well as the optical properties of the Ni, Pd and Pt series are very different from those of the Au complexes. The first series exhibit a strong absorption band in the NIR region while the gold complexes absorb only in the UV–vis range. The monoanionic gold complexes are more difficult to oxidize into the neutral complexes, by about 300 mV when compared to the Ni, Pd and Pt complexes. Although

this class of complexes was originally explored as molecular conductors, they have recently attracted attention, in particular gold(III) bis (dithiolenes), as anticancer and antimicrobial agents. Herein we have assessed the potential biological activities of these eight metal bis (dithiolene) complexes as anticancer and antitrypanosomatid agents. The nature of the alkyl groups does not influence the cytotoxic or antitrypanosomatid properties of this class of transition metal complexes. However, those with the bulkiest substituent on the dithiolene backbone show improved selectivity for T. cruzi trypomastigotes and these complexes present indeed high antiparasitic activity comparable to NFX. As anticancer agents, they present the ability to combat ovarian cancer as well as to overcome resistance in cisplatin-resistant cells. The mechanism of cell death seemed to be mediated mainly by ROS, but further studies are needed to better understand their biological activity. So far, the [P][PttBu] and [P][PdtBu] complexes showed biological profiles that encourage their further exploitation as drug leads for the development of novel molecules with antitumor, and antiparasitic activities as alternatives to the current pharmacological interventions.

CRediT authorship contribution statement

Hadi Hachem: Validation, Investigation. Yann Le Gal: Validation, Investigation. Olivier Jeannin: Formal analysis, Data curation. Dominique Lorcy: Writing – review & editing, Investigation, Conceptualization. Gonzalo Scalese: Validation, Investigation. Leticia Pérez-Díaz: Investigation, Formal analysis. Dinorah Gambino: Writing – review & editing, Conceptualization. António P. Matos: Investigation. Fernanda Marques: Writing – review & editing, Methodology, Investigation, Conceptualization.

Declaration of competing interest

Lorcy Dominique reports was provided by UNMR CNRS-Université de Rennes. If there are other authors, they declare that they have no known competing financial interests or personal relationships that could have appeared to influence the work reported in this paper.

Data availability

Data will be made available on request.

Acknowledgements

This work was supported by the Université de Rennes 1 (pH. D. grant for H Hachem). Marques F. thanks the financial support from Fundacão para a Ciência e Tecnologia (FCT) through project UID/Multi/04349/2019. GS and DG thank PEDECIBA Química of Uruguay.

Appendix A. Supplementary data

Supplementary data to this article can be found online at https://doi.org/10.1016/j.jinorgbio.2024.112788.

References

- [1] J. Spencer, B. Walden, Special focus: metals in medicine, Future Med. Chem. 10 (2018) 607–609, https://doi.org/10.4155/fmc-2018-9999.
- [2] C. Riccardi, M. Piccolo, Metal-based complexes in cancer, Int. J. Mol. Sci. 24 (2023) 7289. https://doi.org/10.3390/jims24087289.
- [3] S. Dasari, P.B. Tchounwou, Cisplatin in cancer therapy: molecular mechanisms of action, Eur. J. Pharmacol. 740 (2014) 364–378, https://doi.org/10.1016/j. ejphar.2014.07.025.
- [4] C. Zhang, C. Xu, X. Gao, Q. Yao, Platinum-based drugs for cancer therapy and antitumor strategies, Theranostics 12 (2022) 2115–2132, https://doi.org/10.7150/ thpo.69424
- [5] T. Lazarević, A. Rilak, Ž.D. Bugarčić, Platinum, palladium, gold and ruthenium complexes as anticancer agents: current clinical uses, cytotoxicity studies and future perspectives, Eur. J. Med. Chem. 142 (2017) 8–31, https://doi.org/ 10.1016/j.ejmech.2017.04.007.

- [6] R.L. Lucaciu, A.C. Hangan, B. Sevastre, L.S. Oprean, Metallo-drugs in cancer therapy: past, present and future, Molecules 27 (2022) 6485, https://doi.org/ 10.3390/molecules/27196485
- [7] C. Jacqueline, A. Tasiemski, G. Sorci, et al., Infections and cancer: the "fifty shades of immunity" hypothesis, BMC Cancer 17 (2017) 257, https://doi.org/10.1186/ s12885-017-3234-4.
- [8] S.Y. Lee, C.Y. Kim, T.G. Nam, Ruthenium complexes as anticancer agents: a brief history and perspectives, Drug Des. Devel. Ther. 14 (2020) 5375–5392, https://doi. org/10.2147/DDDT.S275007.
- [9] C. Nardon, N. Pettenuzzo, D. Fregona, Gold complexes for therapeutic purposes: an updated patent review (2010-2015), Curr. Med. Chem. 23 (2016) 3374–3403, https://doi.org/10.2174/0929867323666160504103843.
- [10] C.I. Yeo, K.K. Ooi, E.R.T. Tiekink, Gold-based medicine: a paradigm shift in anticancer therapy? Molecules 23 (2018) 1410, https://doi.org/10.3390/ psplog/39041410.
- [11] Y. Lu, X. Ma, X. Chang, et al., Recent development of gold(I) and gold(III) complexes as therapeutic agents for cancer diseases, Chem. Soc. Rev. 51 (2022) 5518–5556, https://doi.org/10.1039/d1cs00933h.
- [12] B.D. Glišić, M.I. Djuran, Gold complexes as antimicrobial agents: an overview of different biological activities in relation to the oxidation state of the gold ion and the ligand structure, Dalton Trans. 43 (2014) 5950–5969, https://doi.org/ 10.1039/c4dt00022f.
- [13] L. Feng, S. Pomel, P. Latre de Late, et al., Repurposing auranofin and evaluation of a new gold(I) compound for the search of treatment of human and cattle parasitic diseases: from protozoa to helminth infections, Molecules 25 (2020) 5075, https:// doi.org/10.3390/molecules25215075.
- [14] Y. Liu, Y. Lu, Z. Xu, et al., Repurposing of the gold drug auranofin and a review of its derivatives as antibacterial therapeutics, Drug Discov. Today 27 (2022) 1961–1973, https://doi.org/10.1016/j.drudis.2022.02.010.
- [15] C. Roder, M.J. Thomson, Auranofin: repurposing an old drug for a golden new age, Drugs R D 15 (2015) 13–20, https://doi.org/10.1007/s40268-015-0083-y.
- [16] L. Massai, L. Messori, N. Micale, et al., Gold compounds as cysteine protease inhibitors: perspectives for pharmaceutical application as antiparasitic agents, BioMetals 30 (2017) 313–320, https://doi.org/10.1007/s10534-017-0007-0.
- [17] E.V. Capparelli, R. Bricker-Ford, M.J. Rogers, et al., Phase I clinical trial results of auranofin, a novel antiparasitic agent, Antimicrob. Agents Chemother. 61 (2016) e01947-16, https://doi.org/10.1128/AAC.01947-16.
- [18] C.I. Yeo, C.H.P. Goh, E.R.T. Tiekink, et al., Antibiotics: a "GOLDen" promise? Coord. Chem. Rev. 500 (2024) 215429 https://doi.org/10.1016/j. ccr.2023.215429.
- [19] V. Murray, H.M. Campbell, A.M. Gero, Plasmodium falciparum: the potential of the cancer chemotherapeutic agent cisplatin and its analogues as anti-malarials, Exp. Parasitol. 132 (2012) 440–443, https://doi.org/10.1016/j.exppara.2012.09.004.
- [20] N.A.E. Nassef, M.A. El-Melegy, E.V. Beshay, et al., Trypanocidal effects of cisplatin alone and in combination with nigella sativa oil on experimentally infected mice with Trypanosoma evansi, Iran. J. Parasitol. 13 (2018) 89–99.
- [21] F. Çelik, S. Şimşek, Parasite and cancer relationship, Turkiye Parazitol. Derg. 46 (2022) 150–162, https://doi.org/10.4274/tpd.galenos.2022.30974.
- [22] L.J. Knoll, D.A. Hogan, J.M. Leong, et al., Pearls collections: what we can learn about infectious disease and cancer, PLoS Pathog. 14 (2018) e1006915, https:// doi.org/10.1371/journal.ppat.1006915.
- [23] B.E. Callejas, D. Martínez-Saucedo, L.I. Terrazas, Parasites as negative regulators of cancer, Biosci. Rep. 38 (2018) BSR20180935, https://doi.org/10.1042/ BSR20180935.
- [24] V. Fernández-Moreira, R.P. Herrera, M.C. Gimeno, Anticancer properties of gold complexes with biologically relevant ligands, Pure Appl. Chem. 91 (2019) 247–269, https://doi.org/10.1515/pac-2018-0901.
- [25] M.Q. Klinkert, V. Heussler, The use of anticancer drugs in antiparasitic chemotherapy, Mini-Rev. Med. Chem. 6 (2006) 131–143, https://doi.org/ 10.2174/138955706775475939.
- [26] S. Urig, K. Fritz-Wolf, R. Reau, et al., Undressing of phosphine gold(I) complexes as irreversible inhibitors of human disulfide reductases, Angew. Chem. Int. Ed. Eng. 45 (2006) 1881–1886, https://doi.org/10.1002/anie.200502756.
- [27] M.A. Comini, L. Flohé, Trypanothione-based redox metabolism of trypanosomatids, in: T. Jager, O. Koch, L. Flohe (Eds.), Trypanosomatid Diseases: Molecular Routes to Drug Discovery, Wiley-Blackwell, Oxford, 2013, pp. 167–199.
- [28] M.R. Ariyanayagam, S.L. Oza, M.L.S. Guther, A.H. Fairlamb, Phenotypic analysis of trypanothione synthetase knockdown in the African trypanosome, Biochem. J. 391 (2005) 425–432, https://doi.org/10.1042/BJ20050911.
- [29] A.C. Mesías, N. Sasoni, D.G. Arias, C.P. Brandán, O.C.F. Orban, C. Kunick, C. Robello, M.A. Comini, N.J. Garg, M.P. Zago, Trypanothione synthetase confers growth, survival advantage and resistance to anti-protozoal drugs in Trypanosoma cruzi, Free Radic. Biol. Med. 130 (2019) 23–34, https://doi.org/10.1016/j. freeradbiomed.2018.10.436.
- [30] V. Olin-Sandoval, Z. González-Chávez, M. Berzunza-Cruz, I. Martínez, R. Jasso-Chávez, I. Becker, B. Espinoza, R. Moreno-Sánchez, E. Saavedra, Drug target validation of the trypanothion pathway enzymes through metabolic modelling, FEBS J. 279 (2012) 1811–1833, https://doi.org/10.1111/j.1742-4658.2012.08557.x.
- [31] S. Wyllie, S.L. Oza, S. Patterson, D. Spinks, S. Thompson, A.H. Fairlamb, Dissecting the essentiality of the bifunctional trypanothione synthetase-amidase in *Trypanosoma brucei* using chemical and genetic methods, Mol. Microbiol. 74 (2009) 529–540, https://doi.org/10.1111/j.1365-2958.2009.06761.x.
- [32] S.A. Sousa, J.H. Leitão, R.A.L. Silva, et al., On the path to gold: Monoanionic au bisdithiolate complexes with antimicrobial and antitumor activities, J. Inorg. Biochem. 202 (2020) 110904, https://doi.org/10.1016/j.jinorgbio.2019.110904.

- [33] D. Fontinha, S.A. Sousa, T.S. Morais, et al., Gold(iii) bis(dithiolene) complexes: from molecular conductors to prospective anticancer, antimicrobial and antiplasmodial agents, Metallomics 12 (2020) 974–987, https://doi.org/10.1039/ d0mt00064e.
- [34] Y. Le Gal, A. Filatre-Furcate, D. Lorcy, et al., Broad Spectrum functional activity of structurally related monoanionic au(III) Bis(Dithiolene) complexes, Int. J. Mol. Sci. 23 (2022) 7146, https://doi.org/10.3390/ijms23137146.
- [35] J.F. Santos, R. Azevedo, M. Prudêncio, et al., Block copolymer micelles encapsulating au(III) bis(dithiolene) complexes as promising nanostructures with antiplasmodial activity, Pharmaceutics 15 (2023) 1030, https://doi.org/10.3390/ pharmaceutics15031030.
- [36] C.W. Ang, A.M. Jarrad, M.A. Cooper, M.A.T. Blaskovich, Nitroimidazoles: molecular fireworks that combat a broad spectrum of infectious diseases, J. Med. Chem. 60 (2017) 7636–7657, https://doi.org/10.1021/acs.jmedchem.7b00143.
- [37] N. Tenn, N. Bellec, O. Jeannin, et al., A single-component molecular metal based on a thiazole dithiolate gold complex, J. Am. Chem. Soc. 131 (2009) 16961–16967, https://doi.org/10.1021/ia907426s.
- [38] A. Filatre-Furcate, P. Auban-Senzier, M. Fourmigué, T. Roisnel, V. Dorcet, D. Lorcy, Gold dithiolene complexes: easy access to 2-alkylthio-thiazole dithiolate complexes, Dalton Trans. 44 (2015) 15683–15689, https://doi.org/10.1039/ C5DT02534F.
- [39] A. Filatre-Furcate, N. Bellec, O. Jeannin, et al., Radical or not radical: compared structures of metal (M = Ni, au) bis-dithiolene complexes with a thiazole backbone, Inorg. Chem. 53 (2014) 8681–8690, https://doi.org/10.1021/ ic501293z.
- [40] H. Hachem, Z. Xu, N. Bellec, O. Jeannin, P. Auban-Senzier, T. Guizouarn, M. Fourmigué, D. Lorcy, Neutral closed-shell nickel bis(2-alkylthiothiazole-4,5-dithiolate) complexes as single component molecular conductors, Dalton Trans. 47 (2018) 6580–6589, https://doi.org/10.1039/C8DT00818C.
- [41] A. Filatre-Furcate, T. Roisnel, D. Lorcy, Chemical transformation of dithiolene ligands in heteroleptic and homoleptic complexes (M = Ti, Zn, au), J. Organomet. Chem. 819 (2016) 182–188, https://doi.org/10.1016/j.jorganchem.2016.06.033.
- [42] A. Altomare, G. Cascarano, C. Giacovazzo, A. Guagliardi, M.C. Burla, G. Polidori, M. Camalli, SIR92 a program for automatic solution of crystal structures by direct methods optimized for powder data, J. Appl. Crystallogr. 27 (1994) 435–436, https://doi.org/10.1107/S002188989400021X.
- [43] G.M. Sheldrick, Crystal structure refinement with SHELXL, Acta Cryst C71 (2015)
- [44] L.J. Farrugia, WinGX and ORTEP for windows: an update, J. Appl. Crystallogr. 45 (2012) 849–854, https://doi.org/10.1107/S0021889812029111.
- [45] C. Vitré, Y. Le Gal, A. Vacher, T. Roisnel, D. Lorcy, S. Santana, M. Prudêncio, T. Pinheiro, F. Marques, Structure-activity relationship of anticancer and antiplasmodial gold bis(dithiolene) complexes, Dalton Trans. 53 (2024) 11903–11913, https://doi.org/10.1039/d4dt01458h.
- [46] F. Rivas, C. Del Mármol, G. Scalese, et al., New multifunctional Ru(II) organometallic compounds show activity against Trypanosoma brucei and Leishmania infantum, J. Inorg. Biochem. 237 (2022) 112016, https://doi.org/10.1016/j.jinorgbio.2022.112016.
- [47] M. Soba, G. Scalese, F. Casuriaga, et al., Multifunctional organometallic compounds for the treatment of Chagas disease: re(I) tricarbonyl compounds with two different bioactive ligands, Dalton Trans. 52 (2023) 1623–1641, https://doi. org/10.1039/d2dr03869b.
- [48] G. Scalese, I. Machado, F. Salazar, E.L. Coitiño, I. Correia, J.C. Pessoa, L. Pérez-Diaz, D. Gambino, Facing diseases caused by trypanosomatid parasites: rational design of multifunctional oxidovanadium (IV) complexes with bioactive ligands, Front. Chem. Biol. 2 (2024) 1304571, https://doi.org/10.2289/febbi.20231304571
- [49] F. Rivas, C. Del Mármol, G. Scalese, L. Pérez Díaz, I. Machado, O. Blacque, et al., Multifunctional organometallic compounds active against infective trypanosomes: Ru (II) Ferrocenyl derivatives with two different bioactive ligands, Inorg. Chem. 63 (2024) 11667–11687, https://doi.org/10.1021/acs.inorgchem.4c01125.
- [50] G. Scalese, I. Machado, G. Salinas, et al., Heteroleptic oxidovanadium(V) complexes with activity against infective and non-infective stages of trypanosoma cruzi, Molecules 26 (2021) 5375, https://doi.org/10.3390/molecules26175375.
- [51] M. Vieites, P. Smircich, B. Parajón-Costa, J. Rodríguez, et. al. Potent in vitro anti-Trypanosoma cruzi activity of pyridine-2-thiol N-oxide metal complexes having an inhibitory effect on parasite-specific fumarate reductase. J. Biol. Inorg. Chem., 13 (2008) 723–35. doi: https://doi.org/10.1007/s00775-008-0358-7.
- [52] N. Esfandiari, R.K. Sharma, R.A. Saleh, A.J. Jr Thomas, A. Agarwal, Utility of the nitroblue tetrazolium reduction test for assessment of reactive oxygen species production by seminal leukocytes and spermatozoa, J. Androl. 24 (2003) 862–870, https://doi.org/10.1002/j.1939-4640.2003.tb03137.x.
- [53] J.P. Costa, T. Pinheiro, M.S. Martins, et al., Tuning the biological activity of camphorimine complexes through metal selection, Antibiotics 11 (2022) 1010, https://doi.org/10.3390/antibiotics11081010.
- [54] P. Greenspan, E. P. Mayer, S. D. Fowler. Nile red: a selective fluorescent stain for intracellular lipid droplets. J. Cell Biol., 100 (1985) 965–973. doi: https://doi.org/ 10.1083/jcb.100.3.965.
- [55] T. Kusamoto, H. Nishihara, Zero-, one- and two-dimensional bis(dithiolato)metal complexes with unique physical and chemical properties, Coord. Chem. Rev. 380 (2019) 419–439, https://doi.org/10.1016/j.ccr.2018.09.012.
- [56] M.C. Aragoni, M. Arca, F.A. Devillanova, F. Isaia, V. Lippolis, A. Mancini, L. Pala, A.M.Z. Slawin, J.D. Woolins, [M(R-dmet)₂] bis(1,2-dithiolenes): a promising new

- class intermediate between $[M(dmit)_2]$ and $[M(R,R'-timdt)_2]$ (M=Ni, Pd, Pt), Inorg. Chem. 44 (2005) 9610–9612, https://doi.org/10.1021/ic051260q.
- [57] M.C. Aragoni, M. Arca, F.A. Devillanova, F. Isaia, V. Lippolis, A. Mancini, L. Pala, G. Verani, T. Agostinelli, M. Caironi, D. Natali, M. Sampietro, First example of a near-IR photodetector based on neutral [M(R-dmet)₂] bis(1,2-dithiolene) metal complexes, Inorg. Chem. Commun. 10 (2007) 191–194, https://doi.org/10.1016/j.inoche 2006.10.019
- [58] S. Garzon, A.S. Laganà, J. Casarin, et al., Secondary and tertiary ovarian cancer recurrence: what is the best management? Gland Surg. 9 (2020) 1118–1129, https://doi.org/10.21037/gs-20-325.
- [59] K.C. Kurnit, G.F. Fleming, E. Lengyel, Updates and new options in advanced epithelial ovarian cancer treatment, Obstet. Gynecol. 137 (2021) 108–121, https:// doi.org/10.1097/AOG.0000000000000173.
- [60] A. Zoń, I. Bednarek, Cisplatin in ovarian cancer treatment-known limitations in therapy force new solutions, Int. J. Mol. Sci. 24 (2023) 7585, https://doi.org/ 10.3300/jims24087585
- [61] F.H. Abdalbari, E. Martinez-Jaramillo, B.N. Forgie, et al., Auranofin induces lethality driven by reactive oxygen species in high-grade serous ovarian cancer cells, Cancers (Basel) 15 (2023) 5136, https://doi.org/10.3390/cancers1521513
- [62] I. Landini, A. Lapucci, A. Pratesi, et al., Selection and characterization of a human ovarian cancer cell line resistant to auranofin, Oncotarget 8 (2017) 96062–96078, https://doi.org/10.18632/oncotarget.21708.
- [63] H. Mueller, M.U. Kassack, M. Wiese, Comparison of the usefulness of the MTT, ATP, and calcein assays to predict the potency of cytotoxic agents in various human cancer cell lines, J. Biomol. Screen. 9 (2004) 506–515, https://doi.org/10.1177/ 1087057104265386
- [64] S. Machana, N. Weerapreeyakul, S. Barusrux, A. Nonpunya, B. Sripanidkulchai, T., Thitimetharoch cytotoxic and apoptotic effects of six herbal plants against the human hepatocarcinoma (HepG2) cell line, Chin. Med. 31 (2011) 39, https://doi. org/10.1186/1749-8546-6-39.
- [65] D. Gambino, L. Otero, Metal compounds in the development of antiparasitic agents: rational design from basic chemistry to the clinic, Met. Ions Life Sci. (2019), https://doi.org/10.1515/9783110527872-019.
- [66] M.Q. Klinkert, V. Heussler, The use of anticancer drugs in antiparasitic chemotherapy, Mini-Rev. Med. Chem. 6 (2006) 131–143, https://doi.org/ 10.2174/138955706775475939.
- [67] S. Patterson, S. Wyllie, Nitro drugs for the treatment of trypanosomatid diseases: past, present, and future prospects, Trends Parasitol. 30 (2014) 289–298, https://doi.org/10.1016/j.pt.2014.04.003.
- [68] M.L. Bolognesi, Sustainable anti-trypanosomatid drugs: an aspirational goal for medicinal chemistry, Annu. Rep. Med. Chem. 52 (2019) 153–176, https://doi.org/ 10.1016/bs.armc.2019.05.003.
- [69] L. Gambino, Otero, facing diseases caused by trypanosomatid parasites: rational design of Pd and Pt complexes with bioactive ligands, Front. Chem. 9 (2022) 816266. https://doi.org/10.3389/fchem.2021.816266.
- [70] A.L. Mazzeti, P. Capelari-Oliveira, M.T. Bahia, et al., Review on experimental treatment strategies against trypanosoma cruzi, J. Exp. Pharmacol. 13 (2021) 409–432, https://doi.org/10.2147/JEP.S267378.
- [71] G. Scalese, I. Machado, I. Correia, J.C. Pessoa, L. Bilbao, L. Pérez-Diaz, D. Gambino, Exploring oxidovanadium(iv) homoleptic complexes with 8-hydroxyquinoline derivatives as prospective antitrypanosomal agents, New J. Chem. 43 (2019) 17756–17773.
- [72] J. Kim, H.S. Kim, Y.R. Seo, Understanding of ROS-inducing strategy in anticancer therapy, Oxidative Med. Cell. Longev. 2019 (2019) 5381692, https://doi.org/ 10.1155/2019/5381692
- [73] G.J. Maghzal, K.H. Krause, R. Stocker, V. Jaquet, Detection of reactive oxygen species derived from the family of NOX NADPH oxidases, Free Radic. Biol. Med. 53 (2012) 1903–1918, https://doi.org/10.1016/j.freeradbiomed.2012.09.002.
- [74] H.S. Choi, J.W. Kim, Y.N. Cha, C. Kim, A quantitative nitroblue tetrazolium assay for determining intracellular superoxide anion production in phagocytic cells, J. Immunoass. Immunochem. 27 (2006) 31–44, https://doi.org/10.1080/ 15321810500403722.
- [75] M. Redza-Dutordoir, D.A. Averill-Bates, Activation of apoptosis signalling pathways by reactive oxygen species, Biochim. Biophys. Acta 2016 (1863) 2977–2992, https://doi.org/10.1016/j.bbamcr.2016.09.012.
- [76] M. Brentnall, L. Rodriguez-Menocal, R.L. De Guevara, et al., Caspase-9, caspase-3 and caspase-7 have distinct roles during intrinsic apoptosis, BMC Cell Biol. 14 (2013) 32, https://doi.org/10.1186/1471-2121-14-32.
- [77] K.M. Henkels, J.J. Turchi, Cisplatin-induced apoptosis proceeds by caspase-3dependent and -independent pathways in cisplatin-resistant and -sensitive human ovarian cancer cell lines, Cancer Res. 59 (1999) 3077–3083. PMID: 10397248.
- [78] X. Yang, M. Fraser, M. Abedini, et al., Regulation of apoptosis-inducing factor-mediated, cisplatin-induced apoptosis by Akt, Br. J. Cancer 98 (2008) 803–808, https://doi.org/10.1038/si.bic.6604223.
- [79] Z. Tao, J. Goodisman, H.S. Penefsky, A.K. Souid, Caspase activation by anticancer drugs: the caspase storm, Mol Pharm. 4 (2007) 583–595, https://doi.org/10.1021/ mp070002r
- [80] S. Burattini, E. Falcieri, Analysis of cell death by electron microscopy, Methods Mol Biol. 1004 (2013) 77–89, https://doi.org/10.1007/978-1-62703-383-1_7.
- [81] J. Boren, K.M. Brindle, Apoptosis-induced mitochondrial dysfunction causes cytoplasmic lipid droplet formation, Cell Death Differ. 19 (2012) 1561–1570, https://doi.org/10.1038/cdd.2012.34.
- [82] E. Jarc, T. Petan, Lipid droplets and the management of cellular stress, Yale J Biol Med. 92 (2019) 435–452. PMID: 31543707.